3002 *Inorg. Chem.* **2010**, *49*, 3002–3010
DOI: 10.1021/ic902524u

Inorganic Chemistry
Article

Spectroscopic and Structural Studies of Difluorophosphoryl Azide $F_2P(O)N_3$, Difluorophosphoryl Isocyanate $F_2P(O)NCO$, and Difluorophosphoric Acid Anhydride, $F_2(O)POP(O)F_2$

Xiaoqing Zeng,[†] Michael Gerken,[†,‡] Helmut Beckers,*[,†] and Helge Willner[†]

[†]*FB C—Anorganische Chemie, Bergische Universität Wuppertal, Gaussstrasse 20, 42097 Wuppertal, Germany.*
[‡]*Permanent address: Department of Chemistry and Biochemistry, the University of Lethbridge, Lethbridge, Alberta T1K 3M4, Canada.*

Received December 18, 2009

Difluorophosphoryl azide, $F_2P(O)N_3$, was fully characterized by ^{19}F, ^{31}P, ^{14}N, and ^{15}N NMR, as well as by IR (gas, Ar-matrix), and Raman (liquid, solid) spectroscopy. For comparison the vibrational spectra of the isoelectronic difluorophosphoryl isocyanate, $F_2P(O)NCO$ was also studied. Both molecules were found to exist as single rotamers in the gas, liquid, and solid states. Their solid-state structures were determined by X-ray crystallography as the rotamers with the P═O bond being *cis* to the pseudohalide groups (with respect to the P—N bond). The $F_2P(O)N_3$ molecule exhibits approximate C_s symmetry (ϕ(O1P1—N1N2) = −0.7(3)°), while $F_2P(O)NCO$ is significantly distorted from C_s symmetry (ϕ(O1P1—N1C1) = −18.9(5)°) because of intermolecular C···O contacts. The crystal structure of difluorophosphoric acid anhydride, $F_2(O)POP(O)F_2$, was also determined, possessing crystallographic C_2 symmetry with the two F_2PO groups slightly staggered by 10.66(7)° along the P···P vector, and a P—O—P angle of 140.89(10)° for the bridging oxygen atom. The experimental results are supported by quantum chemical calculations, and the conformational properties of $F_2P(O)N_3$ and $F_2P(O)NCO$ are discussed.

Introduction

Phosphinyl and phosphoryl azides are used as precursors for generating versatile phosphinyl ($R_2P(O)N$) and phosphoryl nitrenes ($(RO)_2P(O)N$).[1] Organic phosphinyl azides with phenyl substituents are relatively stable and widely used in organic synthesis.[2] In contrast, inorganic phosphoryl azides $X_nP(O)N_{3-n}$ (n = 0−2) are not well characterized because of their limited stabilities. The monoazide $F_2P(O)N_3$ was prepared by Shreeve et al. in 1972; it was characterized by IR, ^{19}F and ^{31}P NMR spectroscopy, and mass spectrometry.[3] Its photochemistry has been recently studied in an Ar-matrix.[4]

Compared to the azides, the isoelectronic isocyanates are usually more stable and show some interesting differences in their conformational and structural properties. Difluorophosphoryl isocyanate, $F_2P(O)NCO$, was first prepared by Olah by fluorination of $Cl_2P(O)NCO$ with SbF_3;[5] later it was prepared by several other methods and unambiguously characterized by IR, ^{19}F, and ^{31}P NMR spectroscopy.[6]

Structures and particularly the conformational properties of azides and isoelectronic isocyanates are of general interest and have been extensively studied by means of vibrational spectroscopy, gas electron diffraction (GED), microwave spectroscopy (MW), photoelectron spectroscopy (PES), as well as X-ray crystallography.[7] Recently, the conformational properties of difluoro azido phosphine, F_2PN_3, have been studied by vibrational spectroscopy and GED.[8] Two rotamers, with the N_3 group being *trans* and *cis* to the bisector of the FPF angle, were found to exist in nearly 1:1 ratio in both gas phase and Ar-matrix. This result is in contrast to that of

*To whom correspondence should be addressed. E-mail: beckers@uni-wuppertal.de.

(1) (a) Platz, M. S. In *Reactive Intermediate Chemistry*; Moss, R. A., Platz, M. S., Jones, M., Jr., Eds.; Wiley: New York, 2004; pp 501−559. (b) Majoral, J.-P. In *Multiple Bonds and Low Coordination in Phosphorus Chemistry*; Regitz, M., Ed.; Georg Thieme: Stuttgart, Germany: 1990. (c) Romanenko, V. D.; Sanchez, M. *Coord. Chem. Rev.* **1997**, *158*, 275–324. (d) Bertrand, G.; Majoral, J.-P.; Baceiredo, A. *Acc. Chem. Res.* **1986**, *19*, 17–23.

(2) (a) Harger, M. J. P.; Shimmin, P. A. *J. Chem. Soc., Perkin Trans. 1* **1993**, 227–232. (b) Harger, M. J. P.; Shimmin, P. A. *Chem. Commun.* **1991**, 1187–1188.

(3) O'Neill, S. R.; Shreeve, J. M. *Inorg. Chem.* **1972**, *11*, 1629–1631.

(4) Zeng, X. Q.; Beckers, H.; Willner, H.; Neuhaus, P.; Grote, D.; Sander, W. *Chem.—Eur. J.* **2009**, *15*, 13466–13473.

(5) Kuhn, S. J.; Olah, G. A. *Can. J. Chem.* **1962**, *40*, 1951–1954.

(6) (a) Roesky, H. W. *Angew. Chem., Int. Ed. Engl.* **1967**, *6*, 90. (b) Glemser, O.; Biermann, U.; Fild, M. *Chem. Ber.* **1967**, *100*, 1082–1086. (c) O'Neill, S. R.; Shreeve, J. M. *J. Fluorine Chem.* **1974**, *3*, 361–366.

(7) See for examples: (a) Schulz, A.; Klapötke, T. M. *Inorg. Chem.* **1997**, *36*, 1929–1933. (b) Tornieporth-Oetting, I. C.; Klapötke, T. M. *Angew. Chem., Int. Ed. Engl.* **1995**, *34*, 511–520. (c) Hausser-Wallis, R.; Oberhammer, H.; Einholz, W.; Paetzold, P. O. *Inorg. Chem.* **1990**, *29*, 3286–3289. (d) Sullivan, J. F.; Durig, D. T.; Durig, J. R.; Cradock, S. *J. Phys. Chem.* **1987**, *91*, 1770–1778.

(8) Zeng, X. Q.; Beckers, H.; Willner, H.; Berger, R.; Mitzel, N. W. manuscript in preparation.

 Published on Web 02/09/2010

the isocyanato molecule F_2PNCO, for which only a C_s symmetric rotamer was found in the gas phase with the NCO group being *trans* to the bisector of the FPF angle.[9] The differences in the conformational properties between F_2PN_3 and F_2PNCO motivated us to investigate the corresponding molecules of phosphorus(V), $F_2P(O)N_3$ and $F_2P(O)NCO$, in which a doubly bonded oxygen atom replaces the lone pair of the phosphorus(III) in F_2PN_3 and F_2PNCO.

In this paper, we present a detailed IR (gas, Ar-matrix) and Raman (liquid, solid) spectroscopic study of $F_2P(O)N_3$ and $F_2P(O)NCO$. The crystal structures of both molecules and that of the precursor compound, $F_2(O)POP(O)F_2$, were compared with the results of quantum chemical calculations.

Experimental Section

Caution! *Covalent azides are in general explosive. Although no explosions were encountered with $F_2P(O)N_3$ during this work, it should be handled with care in small quantities (< 5 mmol) and appropriate safety precautions should be taken especially when working with liquid or solid $F_2P(O)N_3$.*

Synthesis of $F_2P(O)N_3$ and $F_2P(O)NCO$. Difluorophosphoryl azide, $F_2P(O)N_3$, was prepared by the reaction of $F_2P(O)Cl$[10] with NaN_3 according to the reported procedure.[3] For the preparation of ^{15}N-enriched $F_2P(O)N_3$, 1-^{15}N sodium azide (98 atom % ^{15}N, EURISO-TOP GmbH) was used. For the preparation of ^{18}O-enriched $F_2P(O)N_3$, ^{18}O-enriched $F_2P(O)Cl$ (95 atom % ^{18}O) was prepared by treating F_2PCl with $^{18}O_3$ at −150 °C. Difluorophosphoryl isocyanate was prepared by the reaction of $F_2(O)POP(O)F_2$[11] with KOCN as described in the literature.[6a] The purity of $F_4P_2O_3$, $F_2P(O)N_3$, and $F_2P(O)NCO$ was ascertained by ^{19}F and ^{31}P NMR spectroscopy.

$F_4P_2O_3$: ^{19}F NMR: δ = −80.0 ppm (d, $^1J(^{31}P-^{19}F)$ = 1066 Hz); ^{31}P NMR: δ = −39.2 ppm (t).

$F_2P(O)N_3$: ^{19}F NMR: δ = −73.3 ppm (d, $^1J(^{31}P-^{19}F)$ = 1044 Hz); ^{31}P NMR: δ = −15.7 ppm (t); ^{14}N NMR: δ ($F_2P(O)\mathit{N}NN$) = −304.3 ppm (s, $\Delta\nu_{1/2}$ = 349.4 Hz), δ ($F_2P(O)N\mathit{N}N$) = −153.0 ppm (s, $\Delta\nu_{1/2}$ = 15.7 Hz), δ ($F_2P(O)NN\mathit{N}$) = −162.2 ppm (s, $\Delta\nu_{1/2}$ = 52.6 Hz).

$F_2P(O)^{15}NNN/F_2P(O)NN^{15}N$: ^{19}F NMR: δ = −73.2 ppm (m), $^1J(^{31}P-^{19}F)$ = 1044 Hz, $^2J(^{15}N-^{19}F)$ = 16 Hz; ^{31}P NMR: δ = −15.7 ppm (m), $^1J(^{15}N-^{31}P)$ = 6 Hz, $^3J(^{15}N-^{31}P)$ = 3 Hz; ^{15}N NMR: δ ($F_2P(O)^{15}\mathit{N}NN$) = −304.3 ppm (m), δ ($F_2P(O)NN^{15}\mathit{N}$) = −162.2 ppm (d).

$F_2P(O)NCO$: ^{19}F NMR: δ = −70.6 ppm (d, $^1J(^{31}P-^{19}F)$ = 1006 Hz), ^{31}P NMR: δ = −30.4 ppm (t).

Vibrational Spectroscopy. Gas-phase FT-IR spectra in the range 4000−400 cm^{-1} were measured in an IR gas cell (optical path length 20 cm, 0.6 cm thick Si windows) contained in the sample compartment of a Bruker Vector 22 FT-IR spectrometer, with an optical resolution of 2 cm^{-1}, 32 scans were co-added for each spectrum.

Raman spectra of liquids were recorded with a Bruker-Equinox 55 FRA 106/S FT-Raman spectrometer using a 1064 nm Nd:YAG laser (200 mW), and 100 scans were averaged at a resolution of 2 cm^{-1}. Liquid samples were flame-sealed in a 4 mm glass capillary for the measurement. For low-temperature Raman measurements, samples were condensed onto a copper finger at 78 K in a high vacuum.

Matrix IR spectra were recorded on a FT-IR spectrometer (IFS 66v/S Bruker) in reflectance mode using a transfer optic. A KBr beam splitter and an MCT detector were used in the region of 5000 to 550 cm^{-1}. A Ge-coated 6 μm Mylar beam splitter combined with a He(l)-cooled Si bolometer and a CsI window at the cryostat were used in the region of 700 to 180 cm^{-1}. For each spectrum, 200 scans at a resolution of 0.25 cm^{-1} were co-added. The gaseous sample was mixed with argon (1:1000) in a 1 L stainless-steel storage container and then small amounts (ca. 1 mmol) of the mixture were deposited within 30 min onto the cold matrix support (16 K, Rh plated Cu block) in high vacuum. Details of the matrix apparatus have been described elsewhere.[12]

NMR Spectroscopy. NMR spectra were measured in CD_2Cl_2 solution at room temperature in flame-sealed glass tubes (o.d. 0.4 cm, i.d. 0.3 cm, length 15 cm) placed in thin-walled 5-mm NMR tubes on a Bruker Avance 400 spectrometer: ^{19}F NMR (376.5 MHz), ^{31}P NMR (242.9 MHz), ^{14}N NMR (43.4 MHz), and ^{15}N NMR (60.8 MHz). The chemical shifts are referenced to external $CFCl_3$ (^{19}F), H_3PO_4 (^{31}P), and CD_3NO_2 (^{14}N and ^{15}N).

X-ray Crystal Structure Determination. (a). Crystal Growth and Crystal Mounting. Crystals of $F_2P(O)N_3$, $F_2P(O)NCO$, and $F_2(O)POP(O)F_2$ were grown in an L-shaped glass tube (o.d. 0.6 cm, length 20 cm). Small amounts (ca. 20 mg) of the compounds were condensed at −196 °C into the open end of the tube, which was connected to the vacuum line and subsequently flame-sealed. For the crystallization of $F_2P(O)N_3$ and $F_2P(O)NCO$, the end without sample was immersed into an ethanol cold bath at about −90 °C, while the whole setup with cold bath was kept in a refrigerator at −20 °C overnight. For the crystallization of $F_2(O)POP(O)F_2$, an ethanol cold bath at about −40 °C was used, with the setup kept in the refrigerator at −20 °C. The glass tube containing the crystals was cut in a cold nitrogen stream (ca. −70 °C) while maintaining the sample at about −196 °C, and the colorless crystals were quickly transferred into a trough cooled by a flow of cold nitrogen. Crystals of $F_2P(O)N_3$, $F_2P(O)NCO$, and $F_2(O)POP(O)F_2$ having the dimensions $0.156 \times 0.095 \times 0.032$, $0.167 \times 0.041 \times 0.040$, and $0.310 \times 0.046 \times 0.044$ mm^3, respectively, were selected at about −70 °C under the microscope. The crystals were picked with a mounted CryoLoop (Hampton Res.) with a magnetic base using a CrystalWand (Hampton Res.) as a handle. The crystal was transferred to the goniometer using CryoTongs (Hampton Res.) that had been immersed in liquid nitrogen.

(b). Collection and Reduction of X-ray Data. Crystals were centered on an Oxford Diffraction Gemini E Ultra diffractometer, equipped with a 2K × 2K EOS CCD area detector, a four-circle kappa goniometer, sealed-tube Enhanced (Mo) and Enhanced Ultra (Cu) X-ray sources, and an Oxford Instruments Cryojet. For the data collection the Mo source emitting graphite-monochromated Mo−Kα radiation (λ = 0.71073 Å) was used. The diffractometer was controlled by the CrysAlis^{Pro} Graphical User Interface (GUI) software.[13] Diffraction data collection strategies for $F_2P(O)N_3$, $F_2P(O)NCO$, and $F_2(O)POP(O)F_2$ were optimized with respect to complete coverage and consisted of five, two, and three ω scans with a width of 1°, respectively. The data collections for $F_2P(O)N_3$, $F_2P(O)NCO$, and $F_2(O)POP(O)F_2$ were carried out at −138, −138, and −123 °C, respectively, in a 1024 × 1024 pixel mode using 2 × 2 pixel binning. Processing of the raw data, scaling of diffraction data, and the application of an empirical absorption correction was completed by using the CrysAlis^{Pro} program.[13]

(c). Solution and Refinement of the Structure. The solutions were obtained by direct methods which located the positions of all atoms. The final refinement was obtained by introducing anisotropic thermal parameters and the recommended weightings for all atoms. The maximum electron densities in the final difference Fourier map were located near the heavy atoms. All calculations were performed using the SHELXTL-plus package

(9) Rankin, D. W. H.; Cyvin, S. J. *J. Chem. Soc., Dalton Trans.* **1972**, 1277–1286.
(10) Rovnaník, P.; Žák, Z.; Černík, M. *Z. Anorg. Allg. Chem.* **2006**, *632*, 1356–1362.
(11) Robinson, E. A. *Can. J. Chem.* **1962**, *40*, 1725–1729.
(12) Schnöckel, H. G.; Willner, H. In *Infrared and Raman Spectroscopy, Methods and Applications*; Schrader, B., Ed.; VCH: Weinheim, 1994.
(13) *CrysAlisPro*, Version 1.171.33.42; Oxford Diffraction Ltd.: Yarnton, Oxford, U.K., 2009.

for the structure determination and solution refinement and for the molecular graphics.[14] The structure of $F_2P(O)NCO$ was refined as a 77.3%: 23.7% twin (twin law: −1 0 0, 0 −1 0, 0 0 −1).

Computational Details. Structural optimizations were performed using DFT (B3LYP,[15] BP86,[16] MPW1PW91[17]), ab initio (MP2)[18] and complete basis set CBS-QB3 methods.[19] For B3LYP and MP2 calculations, both 6-31G(d) and 6-311+G(3df) basis sets were employed, while for BP86 and MPW1PW91 calculations, only the 6-311+G(3df) basis set was used. Natural bond order (NBO) analysis was performed with the B3LYP method. All the calculations were performed using the Gaussian 03 software package.[20]

Results and Discussion

Theoretical Calculations. The potential energy scans for the internal rotation around the P−N bonds in $F_2P(O)N_3$ and $F_2P(O)NCO$ were performed at the B3LYP/6-311+G(3df) level, by structural optimizations while varying the ϕ(OP−NN) and ϕ(OP−NC) dihedral angles of $F_2P(O)N_3$ and $F_2P(O)NCO$, respectively, from 0° (*cis*) to 180° (*trans*) in steps of 5°. The obtained curves are shown in Figure 1. Two minima corresponding to the *cis* and *trans* rotamers were found with an energy difference of about 6 kJ mol^{-1} for $F_2P(O)N_3$ and $F_2P(O)NCO$. While $F_2P(O)N_3$ has a significant energy barrier between the *trans* and *cis* rotamers, a very shallow *trans*-*cis* rotational barrier (< 1.0 kJ mol^{-1}) was obtained for $F_2P(O)NCO$. The *cis* rotamer is the global minimum for both $F_2P(O)N_3$ and $F_2P(O)NCO$.

Complete structural optimizations for the *cis* and *trans* rotamers of $F_2P(O)N_3$ and $F_2P(O)NCO$ were performed with various DFT (B3LYP, BP86, MPW1PW91), ab initio (MP2), and CBS-QB3 methods. The calculations confirm that both the *cis* and *trans* rotamers of C_s symmetry are true minima on the potential energy surfaces, and that the *cis* rotamers are slightly lower in energy (ca. 6.0 kJ mol^{-1}) for both molecules (Table 1). The optimized structures of C_s symmetric rotamers are shown in Figure 2. Assuming similar entropies for the *cis* and *trans* rotamers, a composition of 10 to 20% of the less stable *trans* is expected to be in equilibrium at room temperature.

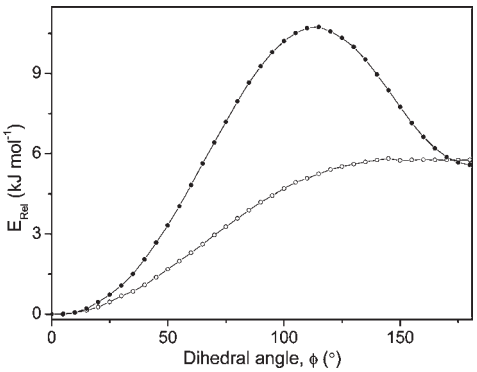

Figure 1. Calculated potential energy curves for internal rotation around the P−N bonds in $F_2P(O)N_3$ (-●-) and $F_2P(O)NCO$ (-○-) at the B3LYP/6-311+G(3df) level. The dihedral angles refer to ϕ(OP−NN) and ϕ(OP−NC) for $F_2P(O)N_3$ and $F_2P(O)NCO$, respectively.

Table 1. Calculated Energy Differences (kJ mol^{-1}), $\Delta E_{trans\text{-}cis}$, at 298 K between the *cis* and the *trans* Rotamers of $F_2P(O)X$ (X = N_3, NCO) at Different Levels of Theory

methods	$F_2P(O)N_3$	$F_2P(O)NCO$
B3LYP/6-31G(d)	5.6	4.0
MP2/6-31G(d)	4.2	3.8
B3LYP/6-311+G(3df)	5.4	5.7
BP86/6-311+G(3df)	4.1	5.4
MPW1PW91/6-311+G(3df)	5.8	5.9
CBS−QB3	6.4	4.4

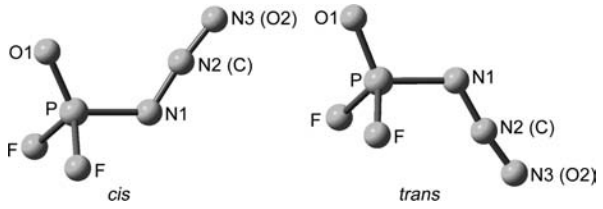

Figure 2. Labeling of the atoms in the two rotamers of $F_2P(O)X$ (X = N_3, NCO).

The calculated structural parameters obtained at the B3LYP/6-311+G(3df) and CBS-QB3 levels for the *cis* and *trans* rotamers of $F_2P(O)N_3$ and $F_2P(O)NCO$ are listed in Table 2 and Table 3, respectively, and the experimental values determined by single-crystal X-ray diffraction (XRD) are also included for comparison. As shown by the experimental dihedral angles, ϕ(O1P−N1N2) and ϕ(O1P−N1C) (Table 2), only the *cis* rotamers of $F_2P(O)N_3$ and $F_2P(O)NCO$, respectively, were obtained in the crystal structures. According to the calculations, the two molecules have very similar structural properties. The main differences are the angles at the bridging nitrogen atom, and a larger angle was predicted for *cis* $F_2P(O)NCO$ ($\angle$(PN1C) = 137.9°) than for *cis* $F_2P(O)N_3$ ($\angle$(PN1N2) = 120.1°). This is in agreement with the XRD data for *cis* $F_2P(O)NCO$ ($\angle$(PN1C) = 132.5°) and *cis* $F_2P(O)N_3$ ($\angle$(PN1N2) = 118.0°).

Vibrational Spectra. Difluorophosphoryl azide was characterized by IR (gas and Ar-matrix) and Raman (liquid and solid) spectroscopy. The IR spectra of gaseous and Ar-matrix-isolated $F_2P(O)N_3$, as well as the Raman spectrum of the liquid are shown in Figure 3. In Table 4 the observed frequencies and IR intensities for the natural-abundant compound are compared to those predicted

(14) Sheldrick, G. M. *SHELXTL97*; University of Göttingen: Göttingen, Germany, 1997.
(15) Becke, A. D. *J. Chem. Phys.* **1993**, *98*, 5648–5652.
(16) Perdew, J. P. *Phys. Rev. B* **1986**, *33*, 8822–8824.
(17) Adamo, C.; Barone, V. *J. Chem. Phys.* **1998**, *108*, 664–675.
(18) Møller, C.; Plesset, M. S. *Phys. Rev.* **1934**, *46*, 618–622.
(19) Montgomery, J. A., Jr.; Frisch, M. J.; Ochterski, J. W.; Petersson, G. A. *J. Chem. Phys.* **2000**, *112*, 6532–6542.
(20) Frisch, M. J.; Trucks, G. W.; Schlegel, H. B.; Scuseria, G. E.; Robb, M. A.; Cheeseman, J. R.; Montgomery, J. A., Jr.; Vreven, T.; Kudin, K. N.; Burant, J. C.; Millam, J. M.; Iyengar, S. S.; Tomasi, J.; Barone, V.; Mennucci, B.; Cossi, M.; Scalmani, G.; Rega, N.; Petersson, G. A.; Nakatsuji, H.; Hada, M.; Ehara, M.; Toyota, K.; Fukuda, R.; Hasegawa, J.; Ishida, M.; Nakajima, T.; Honda, Y.; Kitao, O.; Nakai, H.; Klene, M.; Li, X.; Knox, J. E.; Hratchian, H. P.; Cross, J. B.; Adamo, C.; Jaramillo, J.; Gomperts, R.; Stratmann, R. E.; Yazyev, O.; Austin, A. J.; Cammi, R.; Pomelli, C.; Ochterski, J. W.; Ayala, P. Y.; Morokuma, K.; Voth, G. A.; Salvador, P.; Dannenberg, J. J.; Zakrzewski, V. G.; Dapprich, S.; Daniels, A. D.; Strain, M. C.; Farkas, O.; Malick, D. K.; Rabuck, A. D.; Raghavachari, K.; Foresman, J. B.; Ortiz, J. V.; Cui, Q.; Baboul, A. G.; Clifford, S.; Cioslowski, J.; Stefanov, B. B.; Liu, G.; Liashenko, A.; Piskorz, P.; Komaromi, I.; Martin, R. L.; Fox, D. J.; Keith, T.; Al−Laham, M. A.; Peng, C. Y.; Nanayakkara, A.; Challacombe, M.; Gill, P. M. W.; Johnson, B.; Chen, W.; Wong, M. W.; Gonzalez, C.; Pople, J. A. *Gaussian 03*, revision D.01; Gaussian, Inc.: Wallingford, CT, 2003.

Table 2. Calculated and Experimental Structural Parameters of $F_2P(O)N_3$

	calcd[b]				exptl[d]
	cis		*trans*		
parameter[a]	B3LYP[c]	CBS-QB3	B3LYP[c]	CBS-QB3	XRD
r(P−O1)	1.446	1.447	1.440	1.441	1.442(2)/1.447(2)
r(P−F)	1.545	1.556	1.554	1.566	1.5245(17), 1.5267(18)/1.5234(17), 1.5264(18)
r(P−N1)	1.663	1.666	1.658	1.660	1.639(2)/1.638(2)
r(N1−N2)	1.235	1.239	1.237	1.241	1.255(3)/1.247(3)
r(N2−N3)	1.118	1.122	1.119	1.123	1.113(3)/1.117(3)
∠(O1PN1)	118.6	118.8	114.4	114.6	120.09(12)/120.10(12)
∠(FPO1)	116.3	116.6	116.3	116.6	114.83(11), 115.05(11)/114.66(11), 114.72(11)
∠(FPF)	99.0	98.5	98.6	98.1	98.59(10)/98.96(10)
∠(PN1N2)	120.1	119.6	121.8	121.3	117.31(18)/118.58(19)
∠(N1N2N3)	173.6	173.2	173.4	172.8	173.4(3)/172.4(3)
ϕ(O1P−N1N2)	0.0	0.0	180.0	180.0	−0.2(3)/ −0.7(3)
ϕ(PN1−N2N3)	180.0	180.0	180.0	180.0	179(2)/178(2)

[a] For labeling of the atoms, see Figure 2. [b] Calculated bond lengths (Å) and angles (deg). [c] 6-311+G(3df) basis set was applied. [d] X-ray crystallography.

Table 3. Calculated and Experimental Structural Parameters of $F_2P(O)NCO$

	calcd[b]				exptl[d]
	cis		*trans*		
parameter[a]	B3LYP[c]	CBS-QB3	B3LYP[c]	CBS-QB3	XRD
r(P−O1)	1.444	1.445	1.441	1.442	1.4377(19)
r(P−F)	1.545	1.556	1.550	1.562	1.5195(18)
					1.5166(17)
r(P−N1)	1.637	1.640	1.630	1.634	1.615(2)
r(N−C)	1.211	1.214	1.207	1.213	1.216(3)
r(C−O2)	1.153	1.154	1.154	1.155	1.146(3)
∠(O1PN1)	118.6	118.8	116.1	116.6	119.93(11)
∠(FPO1)	115.9	116.1	115.9	116.1	114.64(12)
					114.33(12)
∠(FPF)	99.6	99.1	99.4	98.8	99.43(12
∠(PN1C)	137.9	136.8	144.9	141.2	132.5(2)
∠(N1CO2)	175.2	175.0	175.4	175.0	174.2(3)
ϕ(O1P−N1C)	0.0	0.0	180.0	180.0	−18.9(5)
ϕ(PN1−CO2)	180.0	180.0	180.0	180.0	174(4)

[a] For labeling of atoms, see Figure 2. [b] Calculated bond lengths (Å) and angles (deg). [c] 6-311+G(3df) basis set was applied. [d] This work.

by B3LYP/6-311+G(3df) calculations. For the strong vibrational modes obtained (gas phase, IR) at 1377 (ν_2), 1280 (ν_3), 917 (ν_4), 963 (ν_{11}), and 551 cm^{-1} (ν_{12}), differences of more than 10 cm^{-1} between the *cis* and *trans* rotamers of $F_2P(O)N_3$ were predicted (Table 4). However, neither the gas-phase IR nor the liquid-state Raman spectra show additional bands with the calculated frequency shifts. The same is true for the matrix IR spectrum (Figure 3, upper trace), where several bands are split by a few wavenumbers because of matrix-site effects. In conclusion, $F_2P(O)N_3$ exists predominantly as the *cis* rotamer. Furthermore, the Raman spectrum of solid $F_2P(O)N_3$ at −196 °C was recorded (Supporting Information, Figure S1). In comparison to the spectrum of the liquid, some bands split in two components as a consequence of the two crystallographically independent $F_2P(O)N_3$ molecules in the unit cell.

Tentative assignments of the fundamental vibrations are made based on predicted band positions and observed $^{14/15}N$ and $^{16/18}O$ isotopic shifts (Table 5). Assuming C_s symmetry for $F_2P(O)N_3$, the 15 normal modes of vibration correspond to the irreducible representations 10 A′ + 5 A″ for the in-plane and out-of-plane

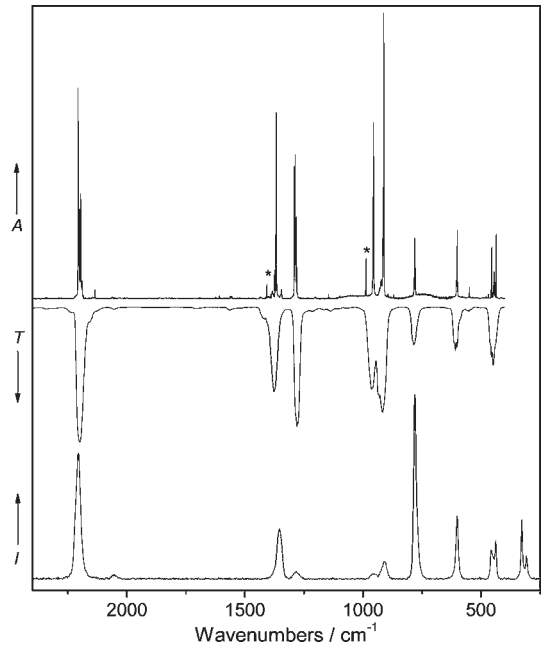

Figure 3. Upper trace: IR spectrum of $F_2P(O)N_3$ isolated in an Ar-matrix at 16 K (absorbance A, resolution: 0.25 cm^{-1}). Middle trace: IR spectrum of gaseous $F_2P(O)N_3$ at 300 K (transmission T, resolution: 2 cm^{-1}). Lower trace: Raman spectrum of liquid $F_2P(O)N_3$ at 300 K (Raman intensity I, resolution: 2 cm^{-1}). Bands associated with impurity of F_3PO are marked with *.

modes, respectively. All the vibrational modes are infrared and Raman active.

Several weak IR combination bands and overtones appear in the range of 4000−1000 cm^{-1} (Supporting Information, Figure S2), and most of them can be satisfactorily assigned by binary combination of fundamental vibrations (Table 4). The most intensive gas-phase IR band at 2199 cm^{-1} is assigned to the characteristic "antisymmetric" stretch of the N_3 group (ν_1), which shows a large ^{15}N isotopic shift at the terminal nitrogen ($\Delta\nu(^{14/15}N_t)$ = 25.9 cm^{-1}). The "symmetric" stretch (ν_3) appears at 1280 cm^{-1} in the IR spectrum as a strong band, showing a comparable ^{15}N isotopic shift at the bridging nitrogen ($\Delta\nu(^{14/15}N_b)$ = 26.5 cm^{-1}), and corresponds to a weak Raman band at 1283 cm^{-1}. Similar to the IR spectra

Table 4. Calculated and Experimental Vibrational Frequencies and Intensities of $F_2P(O)N_3$

calcd[a]		exptl[b]				
		IR		Raman[c]		
cis	*trans*	gas, 300 K	Ar-matrix,[c] 16 K	liquid, 300 K	solid, 78 K	assignment
		3596 vw				
		3465 w				$\nu_1 + \nu_3 = 3479$
		3115 vw				$\nu_1 + \nu_4 = 3116$
		2986 w				$\nu_1 + \nu_5 = 2984$
		2799 vw				$\nu_1 + \nu_6 = 2807$
		2743 vw				$2\,\nu_2 = 2754$
		2682 vw				
		2647 vw				$\nu_1 + \nu_7 = 2649$
		2539 w				
		2496 vw, sh				$\nu_3 + 2\,\nu_6 = 2496$
		2341 w				$\nu_2 + \nu_{11} = 2340$
		2241 w, sh				$\nu_3 + \nu_{11} = 2243$
2321 (523)	2306 (496)	2199 vs	2206.2	2206 s	2219, 2207 s	ν_1, $\nu_{as}(N_3)$
		2057 w				$\nu_3 + \nu_5 = 2065$
		1925 vw				$2\,\nu_{11} = 1926$
		1837 vw				$2\,\nu_4 = 1834$
		1705 vw				$\nu_4 + \nu_5 = 1702$
		1567 w				$2\,\nu_5 = 1570$
		1522 vw, sh				$\nu_4 + \nu_6 = 1525$
		1417 w, sh				$\nu_7 + \nu_{11} = 1419$
1384 (214)	1397 (341)	1377 vs	1367.8	1354 m	1341 s	ν_2, ν(PO)
1353 (263)	1340 (219)	1280 vs	1287.3	1283 w	1302, 1280 m	ν_3, $\nu_s(N_3)$
		1214 w, sh				$2\,\nu_6 = 1216$
		1109 vw				$2\,\nu_{12} = 1112$
		1061 vw				$\nu_6 + \nu_7 = 1058$
930 (196)	907 (201)	963 s	955.3	952 w	945 m	ν_{11}, $\nu_{as}(PF_2)$
892 (302)	874 (227)	917 s, br	912.0	911 m	923, 907 m	ν_4, $\nu_s(PF_2)$
764 (60)	756 (24)	785 m	781.1	781 vs	786 vs	ν_5, ν(PN)
612 (55)	615 (73)	608 m	601.1	602 s	601 s	ν_6, i.p. $\delta(N_3)$
576 (5)	587 (8)	551 m	548.9			ν_{12}, o.p. $\delta(N_3)$
451 (36)	445 (35)	450 m	454.9	457 m	464 m	ν_7, $\delta(PF_2)$
437 (31)	435 (31)		444.3	438 m	439 m	ν_{13}, $\rho(PF_2)$
425 (26)	430 (29)		435.8			ν_8, $\omega(PF_2)$
314 (< 1)	314 (< 1)			327 s	331 s	ν_9
289 (< 1)	307 (< 1)			307 m	315, 304 m	ν_{14}
137 (1)	128 (1)				162 s	ν_{10}
36 (< 1)	50 (< 1)					ν_{15}

[a] B3LYP/6-311+G(3df) calculated IR frequencies (cm^{-1}) and intensities (km mol^{-1}) in parentheses. [b] Experimental frequencies (cm^{-1}), band intensities: vs very strong, s strong, m medium strong, w weak, vw very weak, sh shoulder, and br broad. [c] Most intensive matrix site. [d] Assignments were made according to *cis* $F_2P(O)N_3$.

Table 5. Experimental IR Isotopic Shifts (cm^{-1}) of Ar-Matrix-Isolated $F_2P(O)N_3$

mode	$\Delta\nu(^{14/15}N_b)$[a]	$\Delta\nu(^{14/15}N_t)$[b]	$\Delta\nu(^{16/18}O)$[c]
ν_1	4.2	25.9	1.5
ν_2	0.9	0.9	39.9
ν_3	26.5	9.5	4.3
ν_{11}	0.0	0.0	0.1
ν_4	0.8	0.6	3.4
ν_5	14.5	1.3	3.0
ν_6	0.0	2.0	0.0
ν_{12}	1.8	3.6	
ν_7	1.0	1.0	
ν_{13}	0.0	0.0	
ν_8	1.5	0.9	

[a] The $^{14/15}N$ isotopic shifts of $F_2P(O)N_3$ relative to $F_2P(O)^{15}N_bNN$. [b] The $^{14/15}N$ isotopic shifts of $F_2P(O)N_3$ relative to $F_2P(O)NN^{15}N_t$. [c] The $^{16/18}O$ isotopic shifts of $F_2P(O)N_3$ relative to $F_2P(^{18}O)N_3$.

of other matrix-isolated azides,[21] the N_3 "antisymmetric" stretching band at 2206.2 cm^{-1} (Ar-matrix) is flanked by satellite bands (Figure 3, upper trace), which can probably be attributed to different matrix sites.

The P=O stretching band ν_2 appears at 1377 (IR) and 1354 cm^{-1} (Raman), and exhibits the largest ^{18}O isotopic shift of 39.9 cm^{-1}. Consistent with a previously proposed linear relationship between the P=O stretching frequency and the Pauling electronegativities of the substituents,[22] the P=O stretching frequency of $F_2P(O)N_3$ is higher than those of $FP(O)(N_3)_2$ (1330 cm^{-1})[3] and $OP(N_3)_3$ (1301 cm^{-1}),[23] but lower than that of F_3PO (1415 cm^{-1}).[24] The remaining valence fundamentals are the antisymmetric PF_2 (ν_{11}), the symmetric PF_2 (ν_4), and the PN (ν_5) stretching modes. Of the two PF_2 stretching modes, ν_{11} at 963 cm^{-1} shows no resolved ^{15}N or ^{18}O isotopic shift, while small isotopic shifts were observed for ν_4 at 917 cm^{-1}. The assignment of the PN stretching mode (ν_5) to a rather strong band at 785 cm^{-1} (gas phase) is in account with its considerable $\Delta\nu(^{14/15}N_b)$ of 14.5 cm^{-1}. The bending modes below 785 cm^{-1} are more or less coupled. They are assigned based on the calculated

(21) Frankowski, M.; Fox, B. S.; Smith−Gicklhorn, A. M.; Beyer, M. K.; Bondybey, V. E.; Algarra, M.; Costa, M. L. *Low Temp. Phys.* **2003**, *29*, 870–875.

(22) Bell, J. V.; Heisler, J.; Tannenbaum, H.; Goldenson, J. *J. Am. Chem. Soc.* **1954**, *76*, 5185–5189.

(23) Buder, W.; Schmidt, A. *Z. Anorg. Allg. Chem.* **1975**, *415*, 263–267.

(24) Shimanouchi, T. *J. Phys. Chem. Ref. Data* **1972**, *6*, 993–1102.

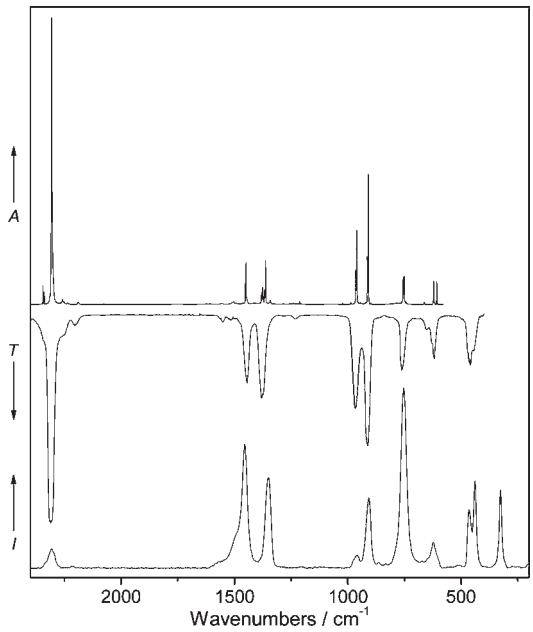

Figure 4. Upper trace: IR spectrum of $F_2P(O)NCO$ isolated in an Ar-matrix at 16 K (absorbance *A*, resolution: 0.25 cm^{-1}). Middle trace: IR spectrum of gaseous $F_2P(O)NCO$ at 300 K (transmission *T*, resolution: 2 cm^{-1}). Lower trace: Raman spectrum of liquid $F_2P(O)NCO$ at 300 K (Raman intensity *I*, resolution: 2 cm^{-1}).

displacement vectors and by comparison with vibrational spectra of similar molecules.

The IR spectra of gaseous and Ar-matrix-isolated $F_2P(O)NCO$, as well as the Raman spectrum of the liquid are shown in Figure 4. In Table 6 the observed frequencies and IR intensities are compared with those predicted from B3LYP/6-311+G(3df) calculations. Tentative assignments of some combination and fundamental bands (Supporting Information, Figure S3) was made by comparison with the IR spectra of F_2PNCO[9] and $F_2P(O)N_3$ (see above). In the gas-phase IR spectrum, the strongest band appeared at 2309 cm^{-1}, which is assigned to the "antisymmetric" stretch of NCO (ν_1). This band coincides with a weak band in the Raman spectrum of the liquid at 2307 cm^{-1}. The "symmetric" stretch (ν_2) is observed at 1445 (IR, gas) and 1455 cm^{-1} (Raman, liquid). The P=O stretching frequency occurred in the gas-phase IR spectrum at 1378 cm^{-1}, very close to that of $F_2P(O)N_3$ (1377 cm^{-1}).

The predicted PN stretching frequencies for the *cis* and *trans* rotamers differ by 24 cm^{-1}. However, only one band was observed in the gas-phase IR and the Raman spectrum of the liquid sample at 761 and 754 cm^{-1}, respectively. On the other hand, three overlapping bands appeared in the matrix IR spectrum at about 750 cm^{-1}. They are likely due to matrix-site splitting (< 3 cm^{-1}). The Raman spectrum of solid $F_2P(O)NCO$ was also recorded (Supporting Information, Figure S4); the observed band splittings are probably due to vibrational coupling of the molecule in the unit cell. Thus, on the basis of the vibrational spectra we conclude that $F_2P(O)NCO$ and $F_2P(O)N_3$ exist predominantly in the energetically more stable *cis* rotamers.

Crystal Structures. The difluorophosphoryl compounds, $F_2P(O)N_3$ and $F_2P(O)NCO$, are liquids at room temperature, and crystals suitable for single-crystal X-ray diffraction were grown by slowly evaporation at −20 °C and condensation at −90 °C in an evacuated L-shaped flame-sealed glass tube. The crystallographic data for both compounds are listed in Table 7.

Difluorophosphoryl azide crystallizes in the triclinic space group $P\bar{1}$ with two crystallographically nonequivalent molecules in the unit cell. As can be seen in Figure 5, $F_2P(O)N_3$ exists only as the *cis* rotamer with essentially C_s symmetry (ϕ(O1PN1N2) = −0.2(3) and −0.7(3)°) in the solid state. The structural parameters for $F_2P(O)N_3$ are listed in Table 2, together with theoretical calculations. The P−O (1.442(2) and 1.447(2) Å) and P−F (1.567(18)−1.5234(17) Å) bonds are slightly longer than those in solid $F_2P(O)Cl$ ($r_{(P-O)}$ = 1.430(3) Å, $r_{(P-F)}$ = 1.514(2) and 1.5161(17) Å).[10]

Difluorophosphoryl isocyanate crystallizes in the tetragonal space group $I\bar{4}$, and the molecular structure is shown in Figure 6. Similar to $F_2P(O)N_3$, $F_2P(O)NCO$ exists only as the *cis* rotamer in the solid state; however, $F_2P(O)NCO$ is considerably distorted from C_s symmetry, as indicated by the dihedral angles ϕ(O1P1−N1C1) = −18.9(3)° and ϕ(P1N1−C1O1) = 174(4)°. The deviation from C_s symmetry is a consequence of intermolecular C···O contacts, as shown in Figure 7, and the fact that deformation of the dihedral angle ϕ(O1P1−N1C1) requires only little energy (Figure 1). These contacts have distances of 2.881(4) and 3.087(4) Å. Both are shorter than the sum of the van der Waals radii for oxygen and carbon (3.22 Å).[25]

The relative electronegativities[26] of Cl > NCO > N_3 result in the lowest positive charge on the phosphorus atom in $F_2P(O)N_3$ and may account for an increase in P−O and P−F bond lengths among $F_2P(O)Cl$, $F_2P(O)NCO$, and $F_2P(O)N_3$. Indeed, the P−O and P−F bond lengths of 1.438(2) and 1.518(2) Å in $F_2P(O)NCO$ are shorter than those of $F_2P(O)N_3$ (Table 2), but still slightly longer than those in $F_2P(O)Cl$.[10]

Crystals of $F_2(O)POP(O)F_2$, which was used as precursor in the synthesis of $F_2P(O)NCO$, were similarly obtained by a slow sublimation at −20 °C. Difluorophosphoric acid anhydride crystallizes in the orthorhombic space group *Pcca*, and the structure is shown in Figure 8. It contains isolated molecules with crystallographic 2-fold symmetry. The two F_2PO moieties are slightly staggered by 10.66(7)° along the P···P vector. The lengths of the P1−O1 and P1−O2 bonds, 1.4312(12) Å and 1.5652(6) Å, respectively, are close to the average P=O double (1.440(1) Å) and P−O single bond lengths (1.570(4) Å) in o'-$(P_2O_5)_\infty$,[27] and the angle at the bridging oxygen atom (O2) in $F_2(O)POP(O)F_2$ (140.89(10)°) is similar to that in o'-$(P_2O_5)_\infty$ (143.7(2)°) as well.[27] The molecular structure of $F_2(O)POP(O)F_2$ is compared with that of solid disulfuryl difluoride, $FS(O)_2OS(O)_2F$.[28] In the solid $FS(O)_2OS(O)_2F$, the two FSO_2 groups are staggered by ϕ(FS−SF) of 144.97(5)°, and an SOS angle of 123.44(7)° was found at the bridging oxygen atom. An increasing XOX angle in the series Cl_2O_7, $S_2O_7^{2-}$,

(25) Bondi, A. *J. Phys. Chem.* **1964**, *68*, 441–451.
(26) (a) Clifford, A. F. *J. Phys. Chem.* **1959**, *63*, 1227–1231. (b) Fluck, E. *Z. Naturforsch.* **1964**, *19b*, 869–872.
(27) Stachel, D.; Svoboda, I.; Fuess, H. *Acta Crystallogr.* **1995**, *C51*, 1049–1050.
(28) Blake, A. J.; Žák, Z. *Acta Crystallogr.* **1993**, *C49*, 7–9.

Table 6. Calculated and Experimental Vibrational Frequencies (cm^{-1}) and Intensities of $F_2P(O)NCO$

calcd[a]		exptl[b]				
		IR		Raman[c]		
cis	*trans*	gas, 300 K	Ar-matrix,[c] 16 K	liquid, 300 K	solid, 78 K	assignment[d]
		3743 w				$\nu_1 + \nu_2 = 3754$
		3684 vw				$\nu_1 + \nu_3 = 3687$
		3225 vw				$\nu_1 + \nu_4 = 3222$
		3074 w				$\nu_1 + \nu_5 = 3070$
		2750 vw				$2\,\nu_3 = 2756$
		2413 w				$\nu_2 + \nu_{11} = 2412$
2379 (1326)	2387 (1366)	2309 vs	2306.9 vs	2307 w	2330, 2292 m	ν_1, ν_{as}(NCO)
		2202 w				$\nu_2 + \nu_5 = 2206$
		2083 vw				$\nu_2 + \nu_6 = 2098$
		1930 vw				$2\,\nu_{11} = 1934$
		1875 vw				$\nu_4 + \nu_{11} = 1880$
		1826 vw				$2\,\nu_4 = 1826$
		1674 vw				$\nu_4 + \nu_5 = 1674$
		1551 w				$\nu_4 + \nu_6 = 1566$
		1519 vw				$2\,\nu_5 = 1522$
1494 (127)	1510 (166)	1445 s	1449.0 m	1455 s	1453 vs	ν_2, ν_s(NCO)
1374 (199)	1388 (220)	1378 s	1363.2 m	1351 s	1340, 1331 m	ν_3, ν(PO)
		1285 vw				
		1234 w				$2\,\nu_{12} = 1238$
		1079 vw				$\nu_7 + \nu_{12} = 1078$
935 (201)	921 (204)	967 s	960.8 s	959 w	948, 937 s	ν_{11}, $\nu_{as}(PF_2)$
887 (293)	874 (242)	913 s	909.5 s	908 s	912 w	ν_4, $\nu_s(PF_2)$
739 (110)	715 (101)	761 s	751.8 m	754 vs	767 vs	ν_5, ν(PN)
630 (50)	626 (55)	653 m sh	621.2 m	623 m	617 s	ν_6, i.p. δ(NCO)
622 (27)	624 (29)	619 m	607.3 m			ν_{12}, o.p. δ(NCO)
456 (46)	453 (43)	459 m br		465 s sh	483, 468 s	ν_7, $\delta(PF_2)$
447 (30)	445 (30)			439 s	44s s	ν_{13}, $\rho(PF_2)$
420 (27)	422 (34)					ν_8, $\omega(PF_2)$
312 (0.4)	313 (0.1)			326 s	338, 331 s	ν_9
310 (0.3)	313 (0.6)					ν_{14}
91 (0.4)	72 (1)					ν_{10}
39 (0.0)	8 (0.5)					ν_{15}

[a] B3LYP/6-311+G(3df) calculated IR frequencies and intensities (km mol^{-1}) in parentheses. [b] Experimental frequencies, and band intensities: vs very strong, s strong, m medium strong, w weak, vw very weak, sh shoulder, and br broad. [c] Most intensive matrix site. [d] Assignments were made according to *cis* $F_2P(O)NCO$.

Table 7. Crystallographic Data of $F_2P(O)N_3$, $F_2P(O)NCO$, and $F_4P_2O_3$

chemical formula	F_2N_3PO	CF_2NPO	$F_4P_2O_3$
space group	$P\bar{1}$(No. 2)	$I\bar{4}$(No. 82)	*Pcca* (No. 54)
a (Å)	5.6202(6)	12.9771(6)	12.3030(8)
b (Å)	5.6798(7)	12.9771(6)	6.4579(3)
c (Å)	12.7182(19)	4.9718(3)	6.4891(3)
α (deg)	97.480(11)	90	90
β (deg)	91.383(10)	90	90
γ (deg)	90.140(9)	90	90
V (Å^3)	402.41(9)	837.27(8)	515.57(5)
Z (molecules/unit cell)	4	8	4
mol wt	127.00	126.99	185.94
calculated density (g cm^{-3})	2.096	2.015	2.395
T (°C)	−138	−138	−123
μ (mm^{-1})	0.601	0.582	0.601
R_1[a]	0.0387	0.0276	0.0262
wR_2[b]	0.0963	0.0550	0.0734

[a] R_1 is defined as $\sum||F_o| - |F_c||/\sum|F_o|$ for $I > 2\sigma(I)$. [b] wR_2 is defined as $[\sum w(F_o^2 - F_c^2)^2/\sum w(F_o^2)^2]^{1/2}$ for $I > 2\sigma(I)$.

$P_2O_7^{4-}$, and $Si_2O_7^{6-}$ (X = Cl, S, P, Si) has been correlated with increasing π contribution in X−O−X bonding,[29] and is consistent with the ligand close packing model.[30] The nonbonded P···P distance in $F_2(O)POP(O)F_2$ (2.9500(5) Å) is close to those in many other compounds

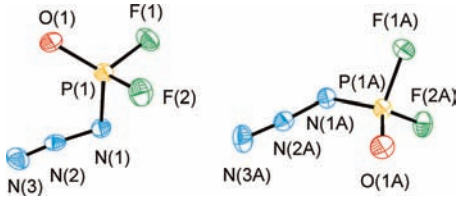

Figure 5. View of the two crystallographically non-equivalent molecules of $F_2P(O)N_3$; thermal ellipsoids are drawn at the 50% probability level.

with two adjacent PF_2 groups attached to O and N atoms.[31]

Theoretical calculations performed for $F_2(O)POP(O)F_2$ predict two rotamers shown in Figure 9. The optimized structures and relative energies are given in Table 8 and Supporting Information, Table S1, respectively. At the CBS-QB3 level of theory, rotamer I with C_2 symmetry is comparable to the structure obtained by X-ray crystallography. It was calculated to be 2.0 kJ mol^{-1} lower in energy than the C_s symmetric rotamer II. For rotamer I the two F_2PO groups are predicted to be staggered by 70.5°, and the P−O−P angle at the bridging oxygen atom was calculated to be 130.1°. Instead of these predicted conformations a *quasi* coplanar arrangement of

(29) Gillespie, R. J.; Robinson, E. A. *Can. J. Chem.* **1964**, *42*, 2496–2503.
(30) Robinson, E. A.; Heard, G. L.; Gillespie, R. J. *J. Mol. Struct.* **1999**, *485−486*, 305–319.
(31) Rankin, D. W. H.; Todd, M. R.; Fild, F. *J. Chem. Soc., Dalton Trans.* **1982**, 2079–2083.

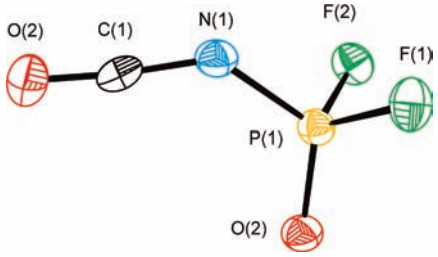

Figure 6. View of the $F_2P(O)NCO$ molecule; thermal ellipsoids are drawn at the 50% probability level.

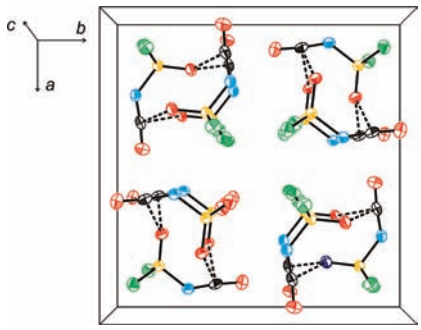

Figure 7. View of the unit cell of $F_2P(O)NCO$ along the *c*-axis. Thermal ellipsoids are drawn at the 50% probability level.

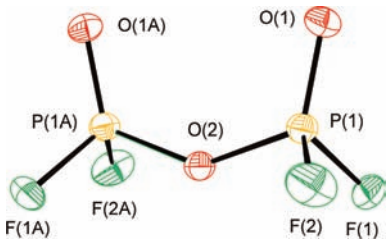

Figure 8. Illustration of the $F_2(O)POP(O)F_2$ molecule with thermal ellipsoids at the 50% probability level.

the (O)POP(O) unit with a dihedral angle ϕ(OPPO) = 10.66(7)° is observed in the solid state. The antiparallel stacking arrangement of the nearly planar central (O)POP(O) units in the solid state structure of $F_2(O)POP(O)F_2$ (Supporting Information, Figure S6) benefits from both, the calculated low-energy difference between the predicted minimum-energy structures and a cancellation of the molecular dipole moments.

Conformational Properties of $F_2P(O)N_3$ and $F_2P(O)NCO$. Although there are numerous studies on syntheses and application of phosphoryl pseudohalides, particularly isocyanates, $X_2P(O)NCO$, and azides, $X_2P(O)N_3$, we are not aware of any studies on their conformational properties. On the other hand, there are still lively discussions about the structures of the related carbonyl[32] and silylisocyanates,[33] XC(O)NCO and X_3SiNCO, respectively. The conformation of these pseudohalides are

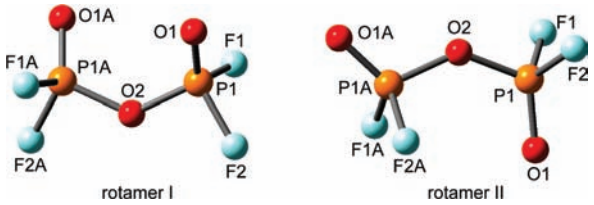

Figure 9. B3LYP/6-311+G(3df) optimized two rotamers of $F_4P_2O_3$.

Table 8. Calculated and Experimental Structural Parameters of $F_4P_2O_3$

	calcd[b]				
	rotamer I		rotamer II		
parameters[a]	B3LYP[c]	CBS-QB3	B3LYP[c]	CBS-QB3	exptl[d]
r(P1−O1)	1.439	1.441	1.437	1.441	1.4312(12)
r(P1−O2)	1.595	1.602	1.592	1.601	1.5652(6)
r(P1−F1)	1.538	1.546	1.540	1.547	1.5109(10)
r(P1−F2)	1.537	1.548	1.540	1.547	1.5125(11)
∠(F1P1F2)	100.5	100.1	100.7	100.0	100.77(7)
∠(O1P1O2)	117.5	117.7	114.3	117.8	119.17(7)
∠(P1O2P1A)	131.7	130.1	135.3	133.9	140.89(10)
ϕ(O1P1−P2O1A)	70.4	70.5	180.0	180.0	10.66(7)

[a] For labeling of the atoms, see Figure 9. [b] Calculated bond lengths (Å) and angles (deg). [c] 6-311+G(3df) basis set was applied. [d] X-ray crystallography.

difficult to predict because of a subtle balance of stabilizing interactions; however, the energetic contributions to these interactions are not readily understood.[33,34]

The present discussion on the phosphoryl pseudohalides may help to unravel some of the conflicting observations,[34] since the conformational properties of the difluorophosphoryl isocyanate and the azide analogue (Figure 1) bear a strong similarity to those of the related fluorocarbonyl, FC(O)NCO[35] and $FC(O)N_3$ derivatives.[35a] In their most stable conformers these pseudohalides adopt a coplanar *cis*-conformation with respect to the E=O bonds (E = P, C). Although this eclipsed arrangement is disfavored by repulsive through-space orbital interaction between the E=O and the pseudohalide substituents, it will be stabilized by electronic interaction, that is, by π-conjugation (utilizing the π-type $\sigma^*(PF_2)$ acceptor orbitals in case of the difluorophosphoryl moiety),[36] as well as by anomeric $n_\sigma(N1) \rightarrow \sigma^*(P-O1)$ donation.[37]

Thus, the *cis*−*trans* barrier can be traced back to the loss of the preferred electronic stabilization by rotation of the pseudohalide out of the molecular plane. However, the energy scan shown in Figure 1 suggests that these electronic effects are more pronounced for the azide rather than for the isocyanato group, since rotation of the isocyanato group around the P1−N1 bond results in a smaller energy change. We may rationalize this feature in terms of the most dominant octet resonance structures

(32) (a) Erben, M. F.; Padró, J. M.; Willner, H.; Della Védova, C. O. *J. Phys. Chem. A* **2009**, *113*, 13029–13035. (b) Al-Saadi, A. A.; Badawi, H. M. *J. Mol. Struct.* (*Theochem*) **2002**, *582*, 11–26. (c) C. O. Klapstein, D.; Nau, W. M. *J. Mol. Struct.* **1993**, *299*, 29–41. (d) McAllister, M. A.; Tidwell, T. T. *J. Chem. Soc. Dalton Trans II*. **1994**, 2239–2248.

(33) (a) Zanchini, C.; Crespini, A. *J. Mol. Struct.* (*Theochem*) **2004**, *682*, 17–27. (b) Palmer, M. H.; Nelson, A. D. *J. Mol. Struct.* **2003**, *660*, 49–65.

(34) (a) Jonas, V.; Frenking, G. *Chem. Phys. Lett.* **1991**, *177*, 175–183. (b) Nguyen, M. T.; Hajnal, M. R.; Vanquickenborne, L. G. *J. Mol. Struct.* (*Theochem*) **1991**, *231*, 185–193. (c) Mack, H.-G; Oberhammer, H.; Della Védova *J. Mol. Struct.* (*Theochem*) **1989**, *200*, 277–288.

(35) (a) Mack, H.-G.; O. Della Védova, C.; Willner, H. *J. Mol. Struct.* **1993**, *291*, 197–209. (b) Durig, J. R.; Guirgis, G. A.; Krutules, K. A.; Phan, H.; Stidham, H. D. *J. Raman Spectrosc.* **1994**, *25*, 221–232.

(36) Reed, A. E.; v. Ragué Schleyer, P. *Inorg. Chem.* **1988**, *27*, 3969–3987.

(37) Reed, A. E.; v. Ragué Schleyer, P. *J. Am. Chem. Soc.* **1990**, *112*, 1434–1445.

Scheme 1. Possible Representations for $F_2P(O)NCO$ (**1a**−**c**) and $F_2P(O)N_3$ (**2a,b**)

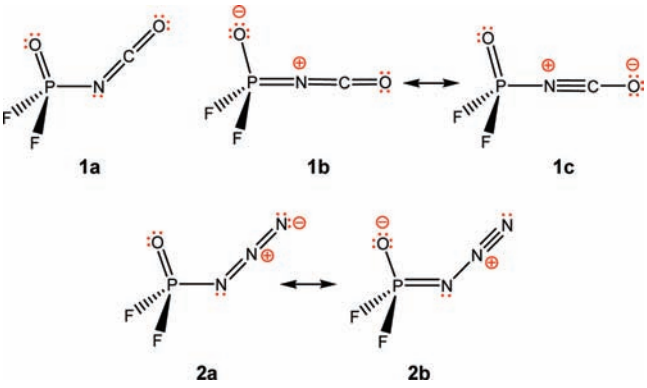

shown in Scheme 1. For the azide one lone-pair of electrons is always retained at the α-N atom in all of these resonance structures (**2a, b**), while this is not the case for those of the isocyanato group (**1a**−**c**). This scheme is supported by the structural data given above for the two fluorophosphoryl pseudohalides, that is, the considerable larger P1N1X (X = N, C) angle and the shorter P1−N1 bond in $F_2P(O)NCO$ (∠(P1N1C1) = 132.5(2)°, *r*(P−N1) = 1.615(2) Å, Table 3) compared to those of $F_2P(O)N_3$ (∠(P1N1N2) = 117.31(18)/118.58(19)°, *r*(P−N1) = 1.639(2)/1.638(2) Å, Table 2). On the other hand, the shorter P1−N1 bond in $F_2P(O)NCO$ can not be attributed to an enhanced π-conjugation or a stronger $n_\sigma(N1) \rightarrow \sigma^*(P-O1)$ hyperconjugation, because the proposed structural changes at the phosphorus center associated with such electronic interactions, that is, increased P−F, and P−O1 bond lengths,[37] respectively, are not observed.

The *cis* over *trans* preference is another intriguing feature of the two fluorophosphoryl pseudohalides. Small *cis*−*trans* energy differences have also been observed for the analogous carbonyl derivatives $XC(O)N_3$ and XC(O)NCO, for which the relative energy ordering depends on the substituent X, for example, for X = F[35] the *cis* conformer is favored, while X = Cl[34] favors the *trans* isomer. The E−F and E−O bonds (E = C and P) are known to have similar σ-acceptor properties,[37] while the steric potential of an oxo group attached to carbon or phosphorus is larger than that of a fluorine ligand.[30] In Supporting Information, Figure S7 calculated dipole moments of the *cis* and *trans* conformers of $F_2P(O)N_3$ and $F_2P(O)NCO$ as well as atomic NBO charges[38] are shown. The dipole moments are lower for the *cis* conformers, since the major dipole contributions (phosphoryl oxygen bond and nitrogen lone pair) point in opposite directions. Furthermore, because of the positive charges centered on the azido nitrogen or the carbon atom of the isocyanato group (Supporting Information, Figure S7), respectively, there will be a stabilizing dipole−dipole interaction between the oppositely charged phosphoryl $P^{\delta+}-O^{\delta-}$ and $N^{\delta-}=X^{\delta+}$ (X = N, C) groups that contribute to the *cis* preference.

(38) Reed, A. E.; Curtiss, L. A.; Weinhold, F. *Chem. Rev.* **1988**, *88*, 899–926.

Conclusions

The present study presents a full characterization of the difluorophosphoryl species, $F_2P(O)N_3$, $F_2P(O)NCO$, and $F_2(O)POP(O)F_2$. According to gas-phase IR, liquid-state Raman, and matrix IR spectroscopic studies these two pseudohalides exist exclusively as the *cis* rotamer in which the oxo and the pseudohalide groups are in a synperiplanar arrangement (with respect to the P−N bond). This is further confirmed by low-temperature single-crystal X-ray diffraction. Calculations using DFT, ab initio, and CBS-QB3 methods predict the *cis* rotamer is more stable than *trans* by about 6.0 kJ mol^{-1}. The *cis* over *trans* preference is ascribed to a subtle balance of stabilizing interactions including electrostatic dipole−dipole interaction; however, further experimental and theoretical work is needed to give a more detailed picture of the energetic contributions that determine the conformational properties of this type of compounds.

The azide $F_2P(O)N_3$ adopts an overall C_s symmetry, while the isocyanate $F_2P(O)NCO$ is considerably distorted from C_s symmetry because of intermolecular interactions in the crystal lattice. The crystal structure of $F_2(O)POP(O)F_2$ contains a C_2-symmetric rotamer, which is in accord with the predicted gas-phase structure.

Acknowledgment. X.Z. expresses his thanks to the Alexander von Humboldt Foundation for a research grant; H.B. and H.W. acknowledge support from the Deutsche Forschungsgemeinschaft and the Fonds der Chemischen Industrie; and M.G. acknowledges the University of Lethbridge for granting a study leave. We are indebted to Prof. R. Eujen and Dr. W. Wiebe for recording the NMR spectra. We are grateful to one of the reviewers who called our attention to the ligand close packing model.

Supporting Information Available: Vibrational spectra of $F_2P(O)N_3$ (Figures S1 and S2); vibrational spectra of $F_2P(O)NCO$ (Figures S3 and S4); vibrational spectra of $F_4P_2O_3$ (Figure S5); calculated energies and a view of the unit cell along the *c*-axis of $F_4P_2O_3$ (Figure S6); calculated dipole moments and NBO charges of $F_2P(O)N_3$ and $F_2P(O)NCO$ (Figure S7). X-ray crystallographic file in CIF format for the structure determinations of $F_2P(O)N_3$, $F_2P(O)NCO$, and $F_4P_2O_3$. This material is available free of charge via the Internet at http://pubs.acs.org.